# Multi-scale structured imaging using wave packets and prolate spheroidal wave functions

*Herwig Wendt*, Maarten V. de Hoop and Fredrik Andersson, Purdue University; Anton Duchkov, IPGG SB RAS*

## SUMMARY

Imaging and inverse scattering of seismic reflection data can be formulated in terms of a certain class of Fourier integral operators. We present an approximation and discretization of such operators following a multi-scale approach, based on wave packets as the quanta for representing seismic data. One of the key ingredients in our approach is the coupling of dyadic parabolic decomposition and prolate spheroidal wave functions. As an example, we detail our method for parametrices of evolution equations, and obtain a one-step algorithm wave-equation for imaging and inverse scattering, time and depth extrapolation, velocity continuation, and extended imaging.

## INTRODUCTION

Wave propagation, downward continuation and imaging can be formulated in terms of members of a certain class of Fourier integral operators, with action on a function $u$ is given by *

$$(Fu)(y) = \int a(y,\xi)\exp(\mathrm{i}S(y,\xi))\hat{u}(\xi)\mathrm{d}\xi. \qquad (1)$$

In the presence of caustics an extension needs to be constructed. We assume here the absence of caustics. The amplitude function $a(y,\xi)$ and the generating function $S(y,\xi) = P(y,\xi) - \langle\xi, y\rangle$ are determined by the ray geometry of the background medium, and the latter describes the propagation of singularities according to de Hoop et al. (2009) $\chi : \left(\frac{\partial S}{\partial \xi}, \xi\right) \rightarrow \left(y, \frac{\partial S}{\partial y}\right)$. $F$ has a sparse matrix representation with respect to the (co-)frame of "wave packets" (Smith (1998), a commonly known instance being the "curvelets", Candès et al. (2006)).
We elaborate on a result in de Hoop et al. (2009), which proposes an approximation of the action of $F$ on a single wave packet with accuracy $\mathscr{O}(2^{-k/2})$ at frequency scale $2^k$ (cf. (4) below), and develop a discrete counterpart for the action of $F$ on a general input function $u$. The method is based on the *multi-scale* expansion of low phase space separation rank of the complex exponential in (1). We express our separated representation in terms of *geometric attributes* of the canonical relation of the FIO: We use *prolate spheroidal wave functions* (PSWFs) in connection with the dyadic parabolic decomposition, while the propagation of singularities is accounted for via an unequally spaced FFT (USFFT). We obtain an algorithm of complexity $\mathscr{O}(DN^d\log(N))$ if $D$ is the number of significant tiles in the dyadic parabolic decomposition. As an example of the FIO in the class considered here, we detail the discrete approximation of solution operators $F$ of evolution equations:

$$[\partial_t + \mathrm{i}P(t,x,D_x)]u = 0, \quad u|_{t=t_0} = u_0, \qquad (2)$$

on the interval $t \in [t_0, \mathscr{T}]$ with symbol $P$ (in the case of the half wave equation, $P = P(x,\xi) = \sqrt{c(x)^2||\xi||^2}$). These operators include wave-equation imaging and inverse scattering, time and depth extrapolation (or downward continuation), velocity continuation, and generate extended imaging.

## OPERATOR EXPANSION AND APPROXIMATION

Let $\varphi_\gamma(x)$, $\gamma = (j,\nu,k)$, denote a wave packet with central position $x_j^{\nu,k}$ and central wave vector $2^k\nu$, that is orientation $\nu$ at scale $k$. We use a result in de Hoop et al. (2009) to obtain an approximation of $(F\varphi_\gamma)(y)$ with accuracy $\mathscr{O}(2^{-k/2})$. The strategy is to replace the phase function $S$ by a sufficient number of terms of its Taylor expansion in $\xi$ on the frequency support of the wave packet $\varphi_\gamma$, $S(y,\xi) \approx \xi\frac{\partial S}{\partial\xi}(y,\nu) + \frac{\xi''^2}{\xi'^2}\cdot\frac{\partial^2 S(y,\nu)}{\partial\xi''^2}$. The first term describes the flow-out of singularities according to geometrical optics and captures the highly oscillatory part of $S$. Let us denote this coordinate transform by

$$y \rightarrow T_{\nu,k}(y) = \frac{\partial S}{\partial\xi}(y,\nu). \qquad (3)$$

Thanks to the parabolic scaling, the second term $\frac{\xi''^2}{\xi'^2}\cdot\frac{\partial^2 S(y,\nu)}{\partial\xi''^2}$ is upper bounded by a constant on the frequency support of $\varphi_\gamma$. By replacing $\exp\left[\mathrm{i}\frac{\xi''^2}{\xi'^2}\cdot\frac{\partial^2 S(y,\nu)}{\partial\xi''^2}\right]$ by a polynomial function, we obtain, to within accuracy $\mathscr{O}(2^{-k/2})$:

$$(F\varphi_\gamma)(y) \approx a(y,\nu)\sum_{r=1}^{R_{\nu,k}}\alpha_{\nu,k}^{(r)}(y)(\vartheta_{\nu,k}^{(r)} * \varphi_\gamma)(T_{\nu,k}(y)), \qquad (4)$$

where $R \sim k/\log(k)$ (de Hoop et al., 2009, Theorem 4.1).

### Prolate spheroidal wave functions

Several approaches have been proposed for expanding the complex exponential in (1) (see e.g. Candès et al. (2007) for a randomized SVD driven numerical procedure, or Wendt et al. (2009), introducing a compressed expansion in orthonormal polynomials). Here, we couple the *dyadic parabolic decomposition* and *prolate spheroidal wave functions* (PSWFs) to obtain the expansion functions $\alpha_{\nu,k}^{(r)}(y)$ and $\vartheta_{\nu,k}^{(r)}$. PSWFs are obtained as the eigenfunctions $\psi_j^c$ of the integral operator with kernel $\exp[\mathrm{i}c\langle x,z\rangle]$ on the unit ball, with corresponding eigenvalues $\lambda_j^c$ (Slepian (1964)), hence reflect the nature of the kernel of (1). We identify the expansion functions:

$$\alpha_{\nu,k}^{(r)}(y) = \psi_r^{c_{\nu,k}}(f_{\nu,k}(y)), \qquad (5)$$

$$\hat{\vartheta}_{\nu,k}^{(r)}(\xi) = \lambda_r^{c_{\nu,k}}\psi_r^c(g_{\nu,k}(\xi)), \qquad (6)$$

where $f_{\nu,k}$ and $g_{\nu,k}$ are suitably chosen transformations form $y$ and $\xi$ to the domain of definition of $\psi_j^c$. This expansion is valid in any dimension. PSWFs are characterized by a rich set of remarkable properties. Among them are the concentration of the energy of their eigenspectrum in a small number of eigenvalues with roughly the same modulus, with exponentially fast decay beyond, and them being at the same time the

*We denote by $\hat{\cdot}$ the Fourier transform of a function, and by $\xi$ the Fourier (frequency) variables.

eigenfunctions of a certain differential operator. The former property guarantees that the number $R_{\nu,k}$ of expansion functions is close to the numerical rank of $\exp\left[\mathrm{i}\frac{\xi''^2}{\xi'}\cdot\frac{\partial^2 S(y,\nu)}{\partial\xi''^2}\right]$ on the frequency support of $\varphi_\gamma$, the latter enables the construction of efficient numerical procedures for their evaluation Xiao et al. (2001). In Fig. 1, we plot the radial parts of several PSWFs for 3 dimensions.

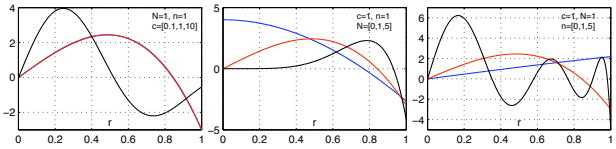


Figure 1: Radial portions of PSWFs of varying order and bandwidth $c$ for $d=3$ dimensions.

## DISCRETIZATION AND COMPUTATION

We denote the discrete data portion corresponding to the frequency box $B_{\nu,k}(\xi)$ in the dyadic parapolic decomposition by:

$$u_{\nu,k}(x_i)=\sum_{\gamma':k'=k,\nu'=\nu} u_{\gamma'}\varphi_{\gamma'}(x_i), \tag{7}$$

where $u_\gamma$ are the coefficients of the wave packet transform. The action of $F$ on $u_{\nu,k}$, evaluated at discrete output points $y_n$, is:

$$(Fu_{\nu,k})(y_n)\approx\sum_{r=1}^{R_{\nu,k}}\alpha_{\nu,k}^{(r)}(y_n)\sum_{\xi_l\in B_{\nu,k}} e^{\mathrm{i}\langle T_{\nu,k}(y_n),\xi_l\rangle}\hat{\vartheta}_{\nu,k}^{(r)}(\xi_l)\hat{u}_{\nu,k}(\xi_l). \tag{8}$$

Our discretization is based on discrete almost symmetric wave packets introduced in Duchkov et al. (2010). This enables us to switch efficiently, via FFTs, between wave packet and and frequency domain representations $u_\gamma$ and $u_{\nu,k}(\xi_l)$, respectively. The action of $F$ on $u_{\nu,k}$ is twofold: enlarged spatial support (wave packets $(\vartheta_{\nu,k}^{(r)}*\varphi_\gamma)(x)$ "spread out") and deformation (under the map $T_{\nu,k}(y)$; this is illustrated in Fig. 2).

In our discretization, we account for this with two additional oversampling factors $\sigma_\xi$ and $\sigma_y$. The first one is directly related to $\frac{\partial^2 S(y,\nu)}{\partial\xi''^2}$ and the parameterization of the wave packet transform geometry and can be compensated by zero-padding, the latter is controlled by $\frac{\partial S(y,\nu)}{\partial\xi}$ and determines the sampling density of the output grid $y_n$.

The sum $\sum_{\xi_l\in B_{\nu,k}}$ in (8) is evaluated by USFFT from the irregularly spaced frequency points $\xi_l$ to the spatial points $x_n=T_{\nu,k}(y_n)$ given by the coordinate transform, which are in general also irregularly spaced ($y_n$ being a regularly spaced grid in order to enable that contributions $(Fu_{\nu,k})(y_n)$ from different boxes $B_{\nu,k}$ can be stacked efficiently to obtain $(Fu)(y_n)\approx\sum_{\nu,k}(Fu_{\nu,k}(y_n))$). In $d$ dimensions, evaluation of (8) requires $\mathcal{O}(R_{\nu,k}N^d\log(N))$ operations, or $\mathcal{O}(N^{\frac{3d-1}{2}}\log(N))$ operations for all boxes in the dyadic parabolic decomposition. Operations per box $B_{\nu,k}$ and tensor product term $r$ can be performed in parallel. Note that the organization in phase-space boxes $B_{\nu,k}$ results in general in a reduction of the calculation domain of (8): $(Fu_{\nu,k})$ needs to be evaluated only at points $y_n$ within the essential spatial support of the wave packets $\varphi_{\gamma':k'=k,\nu'=\nu}$, which is, to precision $\varepsilon$, contained in a volume $\mathcal{O}(2^{-k(d+1)/2})$. This is schematically shown in Fig. 4 (middle, dashed box).

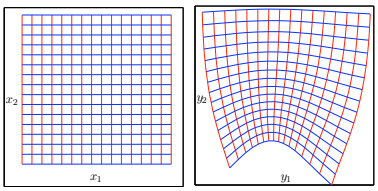


Figure 2: Deformation of discrete grid under $T_{\nu,k}$.

## PARAMETRIX OF EVOLUTION EQUATIONS

We consider the application of (8) to the Cauchy initial value problem (2). In this case, the expansion terms $\frac{\partial S(y,\nu)}{\partial\xi}$ and $\frac{\partial^2 S(y,\nu)}{\partial\xi''^2}$ of the phase of the complex exponential are obtained from the solution of a Hamilton-Jacobi system along paraxial rays. Specifically, let $\mathscr{H}$ be the Hamiltonian corresponding to the principal symbol $P'$ of $P$. Then, $T_{\nu,k}(y)$ is obtained by tracing bi-characteristics (rays ) of $\mathscr{H}$, and $\frac{\partial^2 S(y,\nu)}{\partial\xi''^2}$ is given by a combination of sub-blocks of the propagator matrix $\Pi$ of a dynamic ray tracing system for $\mathscr{H}$ in ray-centered coordinates,

$$\frac{\partial^2 S(y,\nu)}{\partial\xi''^2}=-W_1^{-1}W_3,\quad \Pi=\begin{pmatrix} W_1 & W_2\\ W_3 & W_4\end{pmatrix} \tag{9}$$

The resulting computational procedure is a "one-step" algorithm for the evaluation of the solution operator of (8) for (potentially very) large time step $\mathscr{T}$. By it being a one-step procedure, we can adapt the output resolution grid $y_n$ in our discretization *locally* and minimize the number of points of the calculation domain. Also, the method is insensitive to numerical dispersion, while error accumulation is controlled by the accuracy of the eikonal solver used for integrating the (dynamic) ray tracing systems. We note that these procedures have similarities with beam migration (e.g. Hill (2001); Wang et al. (2009)), where coherent data components are extracted and migrated individually. Here, we obtain "beams" as data wave packets which are one-step propagated using a phase-space localized paraxial approximation. We can also form "boxed beams" as data wave packets that share the same frequency scale and dip.

### Wave propagation

We demonstrate the algorithm for propagation of synthetic data in heterogeneous medium under the half wave equation. As a source, we use a band-limited delta at $z=0$, which we obtained by decomposition of a delta-function into wave packets and thresholding wave packets with slopes $p$ outside a certain range $\pm\Delta p$ from horizontal, and with frequency scale differing from a certain scale $2^{k'}$. As the background, we use the low velocity lens model depicted in Fig. 3 (left). The data consist of $256\times256$ samples. We set $\Delta p=20^\circ$, $k'=3=k_{max}-1$ and consider evolution for large time $\mathscr{T}=20s$. Here and below, the numerical precision for the expansion by PSWFs is set to

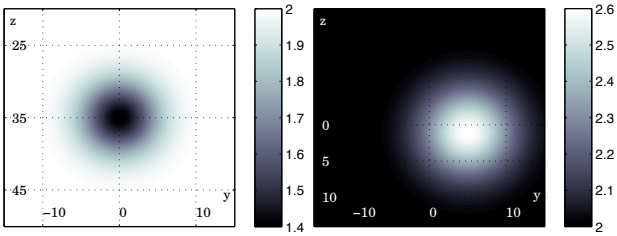


Figure 3: Low velocity lens model (left) and high velocity lens model (right). Units are in $km$ and $km/s$.

$\varepsilon = 10^{-4}$, yielding here on average $R_{\nu,k} \approx 22$ terms. In Fig. 4, we plot the wave front obtained by our algorithm (center). We compare it to a "zero order" approximation (Fig. 4, top) in which we evaluate the coordinate transform $T_{\nu,k}$ only while we set $R_{\nu,k} = 1$ and use expansion functions $\alpha^{(r)}_{\nu,k}(y) = \hat{\vartheta}^{(r)}_{\nu,k}(\xi) = 1$ in (8), yielding accuracy $\mathcal{O}(2^0)$. Fig. 4 (bottom) depicts the corresponding amplitudes along the wave front. The theoretical position of the wave front is indicated by white dots.

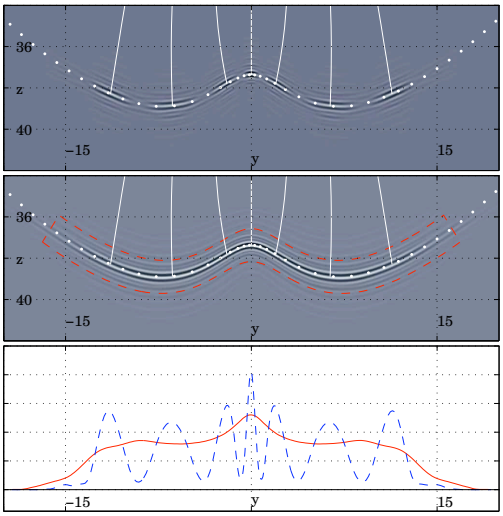


Figure 4: The wave field obtained from a bandlimited delta source by "zero-order" approximation (top) and by using (4) with prolate spheroidal expansion (center). The plot on the bottom depicts the amplitudes along the wave front.

The coordinate transform propagates the wave packets to the right position in the subsurface. The wave front in Fig. 4 (top), produced using coordinate transform $T_{\nu,k}$ only, has large gaps and amplitude fluctuations; this was also observed in Douma and de Hoop (2007). In contrast, with our algorithm, we obtain a very satisfactory image: The wave packets spread out, shear and bend so as to precisely align and connect along the wave front. Similar observations have been reported in Wendt et al. (2009) for an imaging example in homogeneous medium. We note that using all available frequency scales $2^{k'}$ in the data does not improve the image in the zero order approximation, while our algorithm produces the sharp singularity theoretically expected for such a band-limited delta source.

Finally, despite the large evolution time corresponding to propagation for $\approx 160$ wave lengths, we observe no effects of numerical dispersion or error accumulation in Fig. 4.

**Retro-focus and limited aperture array**

Localization in phase space properties are essential in illumination analysis, interferometry, and partial reconstruction and in target-oriented imaging. We illustrate this property for our algorithm in a retro-focus experiment. The synthetic data consist of $512 \times 512$ samples and are one single wave packet $\varphi_\gamma$ at depth $z = 17km$, with vertical wave vector $2^{k'}\nu$ and scale $k' = 4 = k_{max} - 2$ (shown in Fig. 5 (top)). We evaluate

$$(F^*(0,\mathscr{T})(F(0,\mathscr{T})\varphi_\gamma))(x)$$

where $F$ is the solution operator to (2): This means that, first, $\varphi_\gamma$ is propagated upwards to the surface $z = 0$. Then, the so obtained data are again decomposed into wave packets and downwards propagated to depth $z = 17km$. As the background, we use the high velocity lens model depicted in Fig. 3 (right). Fig. 5 (middle) depicts $(F(0,\mathscr{T})\varphi_\gamma)(y)$, the wave field after propagation to the surface: The wave field remains highly localized while being detected by a limited aperture array. Evaluation of $F^*$ on this limited aperture array finally gives the retro-focussed data, which we plot in Fig. 5 (bottom). Comparison with the input data shows that the result of retro-focussing is visually very close; a more detailed analysis reveals that the retro-focussed wave packet essentially preserves the decay properties of $\varphi_\gamma$, while detecting a limited aperture array.

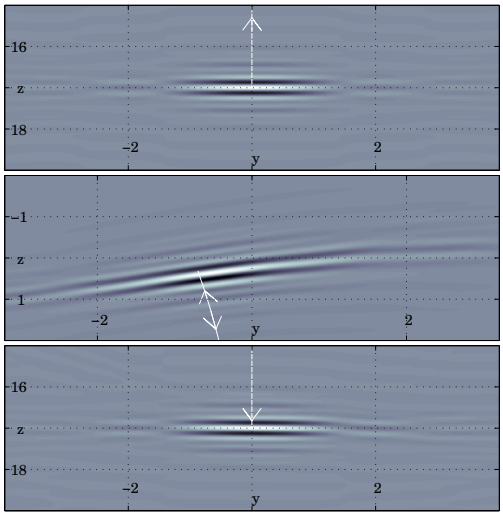


Figure 5: A single wave packet with horizontal slope in the subsurface (top) is upwards propagated to the surface (center). The retro-focussed wave packet obtained by downwards propagation of the wave field in the center plot (bottom).

## IMAGING

We briefly illustrate our approach for zero-offset imaging. We compute post-stack zero-offset images of selected target regions for the synthetic Marmousi data set using a smooth background model. We do not aim at imaging the classical target at

depth $(y,z) = (2.5, 6.5)km$ since we assume here the absence of caustics. The Marmousi model and the four selected target regions are depicted in Fig. 6 (top). The synthetic data consist of $299 \times 1000$ source locations $\times$ time samples, which we interpolate to $512 \times 512$ samples before application of our algorithm, resulting in maximum frequency scale $2^{k_{max}} = 2^5$. Then we decompose the data into wave packets and hard threshold, at each frequency scale $2^k$, wave packet coefficients with magnitude below 10% of the magnitude of the largest coefficient occurring at this scale. The images of the target zones are shown in Fig. 6 (bottom). Our algorithm produces very satisfactory images.

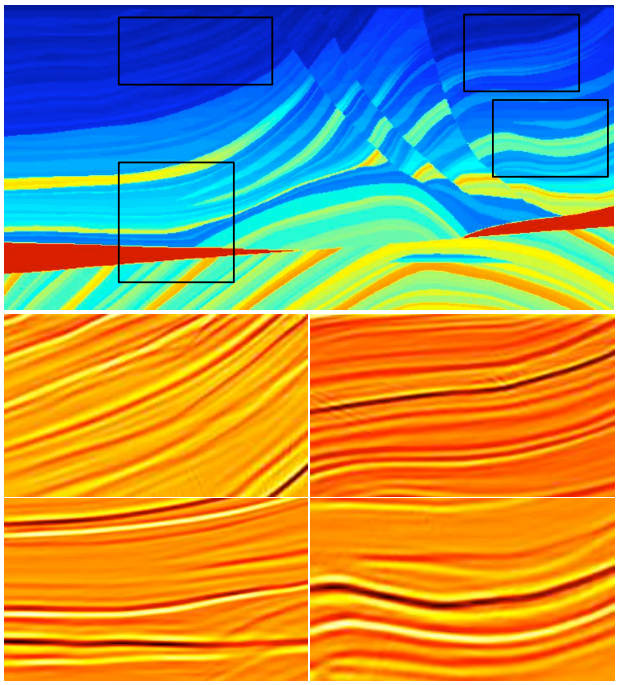

Figure 6: Marmousi model (top) and post-stack zero offset images of 4 target regions, obtained with with our algorithm using a smooth velocity model.

**Trotter product**

The solution operator of (2), $F(\mathscr{T}, t_0)$ say, can be written in form of a Trotter product, resulting in a computational scheme of marching-on-in-time: $\mathscr{W}_N(\mathscr{T}, t_0) = \bar{F}(t, t_N)\,\Pi_{i=N}^{1}\bar{F}(t_i, t_{i-1})$. Each single component operator $\bar{F}$ can by approximated by the "short-time propagator":

$$\bar{F}(t'+\Delta, t')u(t', .)(y) = (2\pi)^{-n} \int \exp[\mathrm{i}\,(P'(t', y, \xi)\Delta - \langle \xi, y\rangle)]\,\hat{u}(t', \xi)\,\mathrm{d}\xi, \quad (10)$$

which is an FIO as in (1), with amplitude $a(y,\xi) = 1$ and phase $S(y,\xi) = P'(t', y, \xi)\Delta - \langle \xi, y\rangle$, where $P'$ is the symbol of $P$. Its canonical transformation $\chi$ describes straight rays in the interval $[t', t'+\Delta]$ and reflects a numerical integration scheme for the Hamilton system, viz., the Euler method; $T_{\nu,k}$ follows from back-tracking straight rays, and the second-order term $\frac{\partial^2 S}{\partial \xi'^2}$ in the expansion of $S$ relates to solving the Hamilton-Jacobi system for paraxial rays. In the case of depth extrapolation, $t$ is replaced by the depth $z$ and $x$ is replaced by the transverse coordinates and time $(x,t)$. The principal symbol of $P$ becomes

$$P'(z,(x,t),(\xi_x,\xi_\tau)) = -\xi_\tau\sqrt{c(z,x)^{-2} - \tau^{-2}|\xi_x|^2},$$
$$S((y,t),(\xi_x,\xi_\tau)) = P'(z',(y,t),(\xi,\tau))\Delta - \langle \xi_x, y\rangle - \xi_\tau t, \quad (11)$$

and $T_{\nu,k}$ and $\frac{\partial^2 S}{\partial \xi'^2}$ are obtained in closed form. The expansion of $S$ yields the (principal) symbol of the paraxial wave equation, *directionally developed relative to* $\nu$, i.e. the orientation of $(\xi_x, \xi_\tau)$. For $\xi_x = 0$, the expression reduces to the standard paraxial 15° approximation $-\xi_\tau c(z', y)^{-1} + \frac{1}{2}\frac{|\xi_x|^2}{\xi_\tau}c(z', y)$; then $T_{\nu,k}$ defines the so-called comoving frame of reference. We refer to the corresponding "short-time" propagator as the "thin-slab" propagator. $\mathscr{W}_N(z, z_0)$ converges in Sobolev operator norm to $F(\mathscr{T}, t_0)$, with convergence rate depending on the Hölder regularity $\alpha$ of $P$ w.r.t. $z$: For $\frac{1}{2} \le \alpha$, it converges as $\mathscr{O}(\Delta^{1/2})$, and balance with $\mathscr{O}(2^{-k/2})$ obtained with our method requires $\Delta \sim 2^{-k}$. We can now construct a process similar to beam migration: We decompose the data into its wave packet components. Each wave packet initializes a solution to the (half-)wave equation, which, through the Trotter product representation, reveals a *phase-space localized* paraxial approximation. The standard paraxial approximation is commonly exploited in beam migration, for example, expressed in terms of geodesic coordinates. In Fig. 7 (left), we show curvilinear coordinates particular to wave packets, which enable to define tubes to which the propagation is confined Fig. 7 (right).

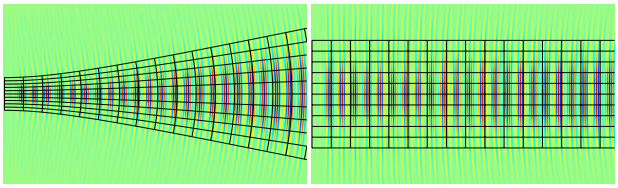

Figure 7: A "beam" of wave packets under (4) for the half-wave equation in homogeneous medium in Cartesian coordinates (left) and elliptic coordinates (right). The elliptic coordinate system is drawn in black in both plots.

## CONCLUSIONS

We introduced a method viewing seismic data through wave packets. This method follows a multi-scale geometric approach and allows us to order and partition the information contained in the data. representations to compress, de-noise and regularize, and to emphasize or mute coherent structures. From these building blocks, we show here how to obtain efficient and effective algorithms for modeling and imaging. One of the key ingredients in our approach is the integration of prolate spheroidal wave functions with the dyadic parabolic decomposition. Our method is valid for general dimension. This approach can be tied to a construction and iteration leading to the full wave solution in velocity models with limited smoothness Andersson et al. (2008).

## REFERENCES


Andersson, F., M. V. de Hoop, H. Smith, and G. Uhlmann, 2008, A multi-scale approach to hyperbolic evolution equations with limited smoothness: Comm. Partial Differential Equations, **33**, 988–1017.

Candès, E., L. Demanet, D. Donoho, and L. Ying, 2006, Fast discrete curvelet transforms: SIAM Multiscale Model. Simul., **5**, 861–899.

Candès, E., L. Demanet, and L. Ying, 2007, Fast computation of fourier integral operators: SIAM J. Sci. Comput., **29**, 2464–2493.

de Hoop, M., H. Smith, G. Uhlmann, and R. van der Hilst, 2009, Seismic imaging with the generalized radon transform: a curvelet transform perspective: Inverse Problems, **25**, 025005+.

Douma, H. and M. de Hoop, 2007, Leading-order seismic imaging using curvelets: Geophysics, **72**, 231–248.

Duchkov, A., F. Andersson, and M. de Hoop, 2010, Discrete almost symmetric wave packets and multi-scale representation of (seismic) waves: IEEE T. Geosci. Remote Sensing, accepted for publication.

Hill, N., 2001, Prestack gaussian beam depth migration: Geophysics, **66**, 1240–1250.

Slepian, D., 1964, Prolate spheroidal wave functions, Fourier analysis and uncertainty–IV: extensions to many dimensions, generalized prolate spheroidal wave functions: Bell Syst. Tech. J., **November**, 3009–3057.

Smith, H., 1998, A parametrix construction for wave equations with $c^{1,1}$ coefficients: Ann. Inst. Fourier, Grenoble, **48**, 797–835.

Wang, B., C. Mason, K. Yoon, J. Ji, J. Cai, and S. Suh, 2009, Complex-salt model building using combination of interactive beam migration and localized rtm: Presented at the Proceedings of SEG.

Wendt, H., M. de Hoop, and F. Andersson, 2009, Multi-scale propagation and imaging with wave packets: Presented at the Proceedings of SEG.

Xiao, H., V. Rokhlin, and N. Yarvin, 2001, Prolate spheroidal wave functions, quadrature and interpolation: Inverse problems, **17**, 805–838.